Soft Matter

Cite this: *Soft Matter*, 2012, **8**, 8223

www.rsc.org/softmatter

PAPER

A constitutive model for coupled fluid permeation and large viscoelastic deformation in polymeric gels

Shawn A. Chester*

Received 19th February 2012, Accepted 24th May 2012
DOI: 10.1039/c2sm25372k

A polymeric gel is a cross-linked polymer network swollen with a solvent. Much of the literature concerning the constitutive response of these materials is limited to elasticity coupled with fluid permeation. We have developed a continuum-level theory to describe the coupled fluid permeation and large viscoelastic deformation of polymeric gels. In discussing special constitutive equations we limit our attention to isothermal conditions, isotropic gels, and consider a model based on a Flory–Huggins model for the free energy change due to mixing of the fluid with the polymer network, coupled with a non-Gaussian statistical–mechanical model for the change in configurational entropy—a model which accounts for the limited extensibility of polymer chains, paired with a linear viscosity. We have numerically implemented our theory in a finite element program. We show that our theory is capable of qualitatively reproducing the experimentally observed behavior of a polymeric gel in simple compression and a fixed depth indentation experiment.

1 Introduction

There are numerous polymeric materials which can absorb large quantities of various solvents without disrupting the underlying polymeric network structure. Such a polymer network, together with the fluid molecules, forms a swollen aggregate called a *gel*. Gels can also be made from colloidal solutions, and such gels are termed colloidal gels. In this paper we restrict our attention to non-ionic polymeric gels.

Early studies of swelling of gels are due to Tanaka and Fillmore[1] and in recent years there have been several notable attempts to formulate a coupled deformation–diffusion theory for describing more complete aspects of the response of gels, including swelling and drying, squeezing of fluid by applied mechanical deformation, and forced permeation.[2–12] We have recently formulated a theory for elastomeric gels.[13,14] Our theory, like most of the other theories referenced above was limited to *elastomeric materials*. Only Korchagin *et al.*[6] has explicitly considered viscoelastic effects, however fluid permeation was not taken into account. Since no real material is completely elastic and will have some amount of dissipation, our objective in this paper is to formulate a constitutive theory for fluid permeation and large viscoelastic deformations in polymeric gels.

In addition to the recent advances in theoretical modeling of gels as mentioned in the previous paragraph, the past decades have seen many contributions from an experimental point of view as well. Scherer[15–19] has been very prolific over the last decades in attempts to characterize gels using various experimental methods from bending to thermal expansion, coupled with a modified Biot[20] *linear poroelastic* analysis to try and obtain material and transport properties of various gels, including viscoelastic gels. More recently, various groups have used indentation and compression,[21–28] again typically coupled with a modified Biot *linear poroelastic* theory to characterize the mechanical and transport properties of the gel. A few recent studies have been undertaken using swelling kinetics[29,30] to try and infer material and transport properties of gels. Examples include, swelling a cantilever consisting of a substrate and a gel and monitoring tip deflection, as well as fluorescence imaging of a swelling gel to measure planar deformation fields.

Most of the literature mentioned in the previous paragraph have used various experimental techniques with the main goal of determining the properties of the material. Ideally, one would put the material into a uniaxial stress state, such as simple compression or simple tension, to obtain its behavior. However, most gels are soft, wet (possibly submerged), and in general difficult to work with in conventional testing machines. Further, many gels lack toughness and fail in simple compression and tension experiments at small to moderate strains.† Nevertheless, a straightforward and accessible experimental method to characterize the behavior of gels is of great interest in the literature. For its simplicity, many researchers have taken to indentation even though the stress, strain, and imbibed solvent concentration fields are inhomogeneous. Due to that inhomogeneity, the main

Engineering Division, Lawrence Livermore National Laboratory, Livermore, CA, USA. E-mail: chester2@llnl.gov

† We note that the most commonly encountered gels are single network gels, which fail relatively easily under mechanical loading. Double network gels have proven to be much tougher and failure resistant[31–33] however, in this paper we consider only single network gels.

challenge is to relate the indentation response (*e.g.*, load-depth, *etc.*) to the properties of the material. Currently the literature is dominated by fully elastic constitutive theories which only exhibit time dependence due to fluid permeation. However, the real material behavior may be time dependent, due to fluid permeation and/or viscoelastic effects. This paper will provide an elementary constitutive theory for viscoelastic polymeric gels so that experimental results may be analyzed and interpreted in a manner that accounts for viscoelastic effects, and not just fluid permeation in time dependent phenomena.

In what follows, we review the basic laws for the balance of forces, the balance of fluid content, and the free energy imbalance; and we formulate a frame-indifferent and thermodynamically consistent coupled deformation–diffusion theory for viscoelastic polymeric gels. In discussing special constitutive equations, we limit our attention to isotropic materials, and consider a model based on the following major ingredients:

(i) First, in the linear theory of viscoelasticity the standard linear solid is the most straightforward and robust model able to capture the two main phenomena of viscoelasticity, stress relaxation and creep. Motivated by the standard linear solid model of linear viscoelasticity, we assume the following kinematical decomposition of the deformation gradient into two micromechanisms,

$$\boldsymbol{F} = \boldsymbol{F}^{(1)} = \boldsymbol{F}^{(2)}.$$

(ii) Second, an essential kinematical ingredient of our theory is the multiplicative decomposition

$$\boldsymbol{F}^{(1)} = \boldsymbol{F}^{e(1)}\boldsymbol{F}^{s}, \text{ with } \boldsymbol{F}^{s} = \lambda^{s}\boldsymbol{1},\ \lambda^{s} > 0,$$

of the deformation gradient $\boldsymbol{F}^{(1)}$ into elastic and swelling parts $\boldsymbol{F}^{e(1)}$ and $\boldsymbol{F}^{s}$, respectively, with the swelling taken to be isotropic, where λ^{s} is the swelling stretch. Additionally, we assume

$$\boldsymbol{F}^{(2)} = \boldsymbol{F}^{e(2)}\boldsymbol{F}^{v},$$

of the deformation gradient $\boldsymbol{F}^{(2)}$ into elastic and viscous parts $\boldsymbol{F}^{e(2)}$ and $\boldsymbol{F}^{v}$, respectively. Correspondingly, with $J = \det \boldsymbol{F} > 0$ denoting the determinant of the deformation gradient, for the first micromechanism we have

$$J = J^{e(1)}J^{s}, \text{ where } J^{e(1)} = \det \boldsymbol{F}^{e(1)} > 0 \text{ and } J^{s} = \det \boldsymbol{F}^{s} = (\lambda^{s})^{3} > 0.$$

The quantity

$$J^{s} - 1$$

represents the change in volume per unit reference volume due to swelling. As in our previous work,[13,14] we assume that this change arises entirely due to the change in the fluid content. Thus, with v denoting the volume of a mole of fluid molecules and c_{R} denoting the number of moles of fluid molecules absorbed by the elastomer per unit volume, we have the important *swelling constraint*

$$J^{s} = 1 + vc_{R}.$$

Additionally, for the second micromechanism we have

$$J = J^{e(2)}J^{v}, \text{ where } J^{e(2)} = \det \boldsymbol{F}^{e(2)} > 0 \text{ and } J^{v} = \det \boldsymbol{F}^{v} > 0$$

We make the important assumption that viscous flow is incompressible,

$$J^{v} = 1$$

Further, we assume that micromechanism 2 has no effect on the volumetric response of the gel, thus the full volumetric response of the gel lies within micromechanism 1.

(iii) Third, we use the Flory[34]–Huggins[35] theory for the free energy change due to mixing of the fluid with the polymer network (*cf.*, *e.g.*, Doi[8,36]). This theory contains a parameter, called the χ-parameter (or interaction parameter), which characterizes the interaction between the solvent and the underlying polymer network.[37]

(iv) Finally, in order to model the change in configurational entropy of the polymer chains we use a non-Gaussian statistical–mechanical model which accounts for the limited extensibility of polymer chains.

We use the numerical implementation consisting of special user-elements which couple mechanical deformation and fluid permeation first described in Chester and Anand[14] in the commercial finite element program Abaqus/Standard.[38] As representative example applications of the theory, we study simple compression and indentation of a finite-dimensioned swollen gel submerged in a solvent.

2 Motivation for the constitutive theory

In the linear theory of viscoelasticity, in a one dimensional setting, one typically connects springs and viscous elements (dashpots) in various combinations to model viscoelastic behavior in the small strain regime. A spring and dashpot connected in series is termed a Maxwell model, and a spring and dashpot connected in parallel is termed a Kevlin–Voigt model. Even in the most simple situations, neither model is acceptable since the Maxwell model cannot accurately describe creep, and the Kelvin–Voigt model cannot accurately describe stress relaxation, the two fundamental phenomena of viscoelasticity. However, the *standard linear solid* is composed of a both of the aforementioned models and consists of a spring in parallel with a Maxwell element. A one dimensional spring–dashpot schematic for the standard linear solid is shown in Fig. 1.

The main kinematical features of this model are (i) that the total strain is the same in each branch, and (ii) the strain in the viscous branch is decomposed into elastic and viscous components,

$$\varepsilon = \varepsilon^{(1)} = \varepsilon^{(2)}, \text{ with } \varepsilon^{(2)} = \varepsilon^{e} + \varepsilon^{v}. \tag{1}$$

Further, the total stress is the sum of the stresses in both branches

$$\sigma = \sigma^{(1)} + \sigma^{(2)}. \tag{2}$$

Typically, the following constitutive relations are implemented

$$\sigma^{(1)} = E_{1}\varepsilon, \tag{3}$$

$$\sigma^{(2)} = E_{2}\varepsilon^{e} = \dot{\varepsilon}^{v}\nu, \tag{4}$$

with E_{1} the modulus of the spring in branch 1, E_{2} the modulus of the spring in branch 2, and ν the viscosity of the dashpot. Combined, the governing equation for the materials response for the standard linear solid may be expressed as

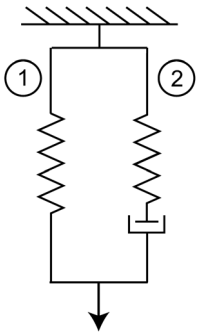

Fig. 1 Schematic of a spring and dashpot rheological model of the standard linear solid. Mechanism 1 is fully elastic, whereas mechanism 2 contains an elastic element and a viscous element.

$$\dot{\varepsilon} = (E_1 + E_2)^{-1}\left(\dot{\sigma} + \frac{E_2}{\nu}\sigma - \frac{E_1 E_2}{\nu}\varepsilon\right), \tag{5}$$

with a characteristic relaxation time $t_r = \nu/E_2$.

The standard linear solid model is the simplest and most widespread model capable of describing the two main phenomena of linear viscoelasticity, namely stress relaxation and creep. In the essence of keeping the constitutive forms simple, in this paper we will use the standard linear solid as motivation for a three dimensional large deformation viscoelastic model for polymeric gels. Of course more refined constitutive models may be implemented for comparison with experimental data, however for our purposes qualitative comparison is satisfactory.

3 Kinematics

Many of the details related to the development of this theory are presented in our previous work, and for that reason, here we present only the new portions to the theory, and give only the results from our previous work. Interested readers are referred to Chester and Anand[13,14] regarding details of our constitutive theory and its development for elastomeric gels in the absence of viscous effects.

Consider a fluid-free (dry) macroscopically homogeneous body. In what follows, the spatially continuous fields that define our continuum theory represent averages meant to apply at length scales which are large compared to the length scales associated with the molecular network and its microscopic-scale free-volume/pore-structure. We identify such a macroscopically homogeneous body B with the region of space it occupies in a fixed *reference configuration*, and denote by $\boldsymbol{X}$ an arbitrary material point of B. A *motion* of B is then a smooth one-to-one mapping $\boldsymbol{x} = \boldsymbol{\chi}(\boldsymbol{X},t)$ with *deformation gradient*, *velocity*, and *velocity gradient* given by:‡

$$\boldsymbol{F} = \nabla\boldsymbol{\chi},\ \boldsymbol{v} = \dot{\boldsymbol{\chi}},\ \boldsymbol{L} = \operatorname{grad}\boldsymbol{v} = \dot{\boldsymbol{F}}\boldsymbol{F}^{-1}. \tag{6}$$

Based on the description of the standard linear solid in the previous section, specifically (1), we base our theory on the following decomposition of the deformation gradient

$$\boldsymbol{F} = \boldsymbol{F}^{(1)} = \boldsymbol{F}^{(2)}, \tag{7}$$

with

$$\boldsymbol{F}^{(1)} = \boldsymbol{F}^{e(1)}\boldsymbol{F}^{s},\ \text{and}\ \boldsymbol{F}^{(2)} = \boldsymbol{F}^{e(2)}\boldsymbol{F}^{v}. \tag{8}$$

Here, micromechanism 1 represents an elastomeric gel identical in form to our previous work,[14] and micromechanism 2 represents a viscoelastic contribution. Based on (7) it may be shown that the Cauchy stress admits the decomposition

$$\boldsymbol{T} = \boldsymbol{T}^{(1)} + \boldsymbol{T}^{(2)}. \tag{9}$$

A micromechanism-type of description (7) and multiplicative decomposition (8) has recently been used successfully in modeling the complex and multi-physics behavior of various polymers.[40–45]

We write

$$J \overset{\text{def}}{=} \det\boldsymbol{F} > 0, \tag{10}$$

and hence, using (7), and (8),

$$J = J^{e(1)}J^{s} = J^{e(2)}J^{v}, \quad \text{where } J^{e(1)} \overset{\text{def}}{=} \det\boldsymbol{F}^{e(1)} > 0,$$

$$J^{s} \overset{\text{def}}{=} \det\boldsymbol{F}^{s} > 0,\ \text{and } J^{e(2)} \overset{\text{def}}{=} \det\boldsymbol{F}^{e(2)} > 0,\ J^{v} \overset{\text{def}}{=} \det\boldsymbol{F}^{v} > 0. \tag{11}$$

Using the notation $\alpha = \{1,2\}$ for brevity, as is standard,

$$\boldsymbol{F} = \boldsymbol{R}\boldsymbol{U} = \boldsymbol{V}\boldsymbol{R}\ \text{and}\ \boldsymbol{F}^{e(\alpha)} = \boldsymbol{R}^{e(\alpha)}\boldsymbol{U}^{e(\alpha)} = \boldsymbol{V}^{e(\alpha)}\boldsymbol{R}^{e(\alpha)}, \tag{12}$$

denote the right and left polar decompositions of $\boldsymbol{F}$ and $\boldsymbol{F}^{e(\alpha)}$, respectively, with $\boldsymbol{U}$, $\boldsymbol{V}$, $\boldsymbol{U}^{e(\alpha)}$ and $\boldsymbol{V}^{e(\alpha)}$ symmetric and positive definite tensors, with $\boldsymbol{R}$ and $\boldsymbol{R}^{e(\alpha)}$ rotations. Also, the tensors

$$\begin{gathered}\boldsymbol{C} = \boldsymbol{U}^2 = \boldsymbol{F}^{\mathsf{T}}\boldsymbol{F},\ \boldsymbol{B} = \boldsymbol{V}^2 = \boldsymbol{F}\boldsymbol{F}^{\mathsf{T}},\ \text{and}\ \boldsymbol{C}^{e(\alpha)} = \boldsymbol{U}^{e(\alpha)2} = \boldsymbol{F}^{e(\alpha)\mathsf{T}}\boldsymbol{F}^{e(\alpha)},\\ \boldsymbol{B}^{e(\alpha)} = \boldsymbol{V}^{e(\alpha)2} = \boldsymbol{F}^{e(\alpha)}\boldsymbol{F}^{e(\alpha)\mathsf{T}},\end{gathered} \tag{13}$$

denote the total and elastic, right and left Cauchy–Green tensors.

Turning our attention to next to micromechanism 2, by $(6)_3$ and $(8)_2$,

$$\boldsymbol{L} = \boldsymbol{L}^{e(2)} + \boldsymbol{F}^{e(2)}\boldsymbol{L}^{v}\boldsymbol{F}^{e(2)-1}, \tag{14}$$

with

$$\boldsymbol{L}^{e(2)} = \dot{\boldsymbol{F}}^{e(2)}\boldsymbol{F}^{e(2)-1},\ \boldsymbol{L}^{v} = \dot{\boldsymbol{F}}^{v}\boldsymbol{F}^{v-1}. \tag{15}$$

As is standard, we define the elastic and viscous stretching and spin tensors through

$$\left.\begin{aligned}\boldsymbol{D}^{e(2)} &= \operatorname{sym}\boldsymbol{L}^{e(2)},\ \boldsymbol{W}^{e(2)} = \operatorname{skw}\boldsymbol{L}^{e(2)},\\ \boldsymbol{D}^{v} &= \operatorname{sym}\boldsymbol{L}^{v},\ \boldsymbol{W}^{v} = \operatorname{skw}\boldsymbol{L}^{v},\end{aligned}\right\} \tag{16}$$

so that $\boldsymbol{L}^{e(2)} = \boldsymbol{D}^{e(2)} + \boldsymbol{W}^{e(2)}$ and $\boldsymbol{L}^{v} = \boldsymbol{D}^{v} + \boldsymbol{W}^{v}$.

‡ Notation: we use standard notation of modern continuum mechanics.[39] Specifically: ∇ and Div denote the gradient and divergence with respect to the material point $\boldsymbol{X}$ in the reference configuration; grad and div denote these operators with respect to the point $\boldsymbol{x} = \boldsymbol{\chi}(\boldsymbol{X},t)$ in the deformed body; a superposed dot denotes the material time-derivative. Throughout, we write $\boldsymbol{F}^{e-1} = (\boldsymbol{F}^{e})^{-1}$, $\boldsymbol{F}^{e-\mathsf{T}} = (\boldsymbol{F}^{e})^{-\mathsf{T}}$, *etc.* We write tr $\boldsymbol{A}$, sym $\boldsymbol{A}$, skw $\boldsymbol{A}$, $\boldsymbol{A}_0$, and $\operatorname{sym}_0\boldsymbol{A}$ respectively, for the trace, symmetric, skew, deviatoric, and symmetric-deviatoric parts of a tensor $\boldsymbol{A}$. Also, the inner product of tensors $\boldsymbol{A}$ and $\boldsymbol{B}$ is denoted by $\boldsymbol{A}{:}\boldsymbol{B}$, and the magnitude of $\boldsymbol{A}$ by $|\boldsymbol{A}| = \sqrt{\boldsymbol{A}{:}\boldsymbol{A}}$.

3.1 Spherical swelling, incompressible irrotational viscous flow

In this section we make some assumptions concerning the deformation of viscoelastic polymeric gels. Starting with micromechanism 1, as most of the literature of polymeric gels does, we assume that the swelling is spherical,

$$\boldsymbol{F}^{(1)} = \boldsymbol{F}^{e(1)}\boldsymbol{F}^{s}, \text{ with } \boldsymbol{F}^{s} = \lambda^{s}\mathbf{1},\ \lambda^{s} > 0. \tag{17}$$

Thus, using $(17)_2$,

$$J^{s} = (\lambda^{s})^{3}. \tag{18}$$

Next, we assume that viscous flow in micromechanism 2 is irrotational and incompressible

$$\boldsymbol{W}^{v} = 0, \text{ and } J^{v} = 1, \tag{19}$$

such that

$$\dot{\boldsymbol{F}}^{v} = \boldsymbol{D}^{v}\boldsymbol{F}^{v}, \text{ with tr } \boldsymbol{D}^{v} = 0. \tag{20}$$

4 Balance laws. Thermodynamics

4.1 Balance of forces and moments

Throughout, we denote by P an arbitrary *part* (subregion) of the reference body B, with $\boldsymbol{n}_{R}$ the outward unit normal on the boundary ∂P of P.

Since time scales associated with fluid diffusion are usually considerably longer than those associated with wave propagation, we neglect all inertial effects. Then, standard considerations of balance of forces and moments, when expressed referentially, give:

(a) There exists a stress tensor $\boldsymbol{T}_{R}$, called the Piola stress, such that the surface traction on an element of the surface ∂P of P, is given by

$$\boldsymbol{t}_{R}(\boldsymbol{n}_{R}) = \boldsymbol{T}_{R}\boldsymbol{n}_{R}. \tag{21}$$

(b) $\boldsymbol{T}_{R}$ satisfies the macroscopic force balance

$$\text{Div } \boldsymbol{T}_{R} + \boldsymbol{b}_{R} = 0, \tag{22}$$

where $\boldsymbol{b}_{R}$ is an external body force per unit reference volume, which, consistent with neglecting inertial effects, is taken to be time-independent.

(c) $\boldsymbol{T}_{R}$ obeys the symmetry condition

$$\boldsymbol{T}_{R}\boldsymbol{F}^{\top} = \boldsymbol{F}\boldsymbol{T}_{R}^{\top}, \tag{23}$$

which represents a balance of moments.

Finally, as is standard, the Piola stress $\boldsymbol{T}_{R}$ is related to the standard symmetric Cauchy stress $\boldsymbol{T}$ in the deformed body by

$$\boldsymbol{T}_{R} = J\boldsymbol{T}\boldsymbol{F}^{-\top}, \tag{24}$$

so that

$$\boldsymbol{T} = J^{-1}\boldsymbol{T}_{R}\boldsymbol{F}^{\top}.$$

4.2 Balance law for the fluid content. Swelling constraint

Let

$$c_{R}(\boldsymbol{X},t) \tag{26}$$

denote the number of moles of fluid molecules absorbed by the polymer network, reckoned per unit volume of the dry reference configuration. We call c_{R} the fluid content.§

Define a *fluid flux* $\boldsymbol{j}_{R}$, measured per unit area, per unit time, so that $-\int_{\partial P}\boldsymbol{j}_{R}\cdot\boldsymbol{n}_{R}\,da_{R}$ represents the number of moles of fluid molecules entering P across ∂P, per unit time. In this case the *balance law for fluid content* takes the form

$$\dot{c}_{R} = -\text{Div } \boldsymbol{j}_{R}. \tag{27}$$

Now,

$$J^{s} - 1 \tag{28}$$

represents the change in volume per unit reference volume due to swelling. *We assume that this change arises entirely due to the change in the fluid content*, so that with v denoting the volume of a mole of fluid molecules we have the important *swelling constraint*

$$J^{s} = 1 + vc_{R}. \tag{29}$$

Note that on account of (18), the constraint (29) may also be stated as

$$\lambda^{s} = (1 + vc_{R})^{1/3}. \tag{30}$$

4.3 Free energy imbalance

Under isothermal conditions the free energy imbalance represents the first two laws of thermodynamics. The imbalance requires that the temporal increase in free energy of any part be less than or equal to the power expanded on that part plus the free energy carried into that part by fluid transport. Thus, with ψ_{R} denoting the free energy per unit reference volume, the free energy imbalance takes the form

$$\dot{\int_{P}}\psi_{R}\,dv_{R} \le \int_{\partial P}(\boldsymbol{T}_{R}\boldsymbol{n}_{R})\cdot\dot{\boldsymbol{\chi}}\,da_{R} + \int_{P}\boldsymbol{b}_{R}\cdot\dot{\boldsymbol{\chi}}\,dv_{R} - \int_{\partial P}\mu\boldsymbol{j}_{R}\cdot\boldsymbol{n}_{R}\,da_{R}, \tag{31}$$

where the last term in (31) represents the flux of energy carried into P by the flux $\boldsymbol{j}_{R}$ of fluid molecules and μ the chemical potential.

Upon use of the balance laws (22) and (27), and using the fact that (31) must hold for all parts P, gives the local form of the energy balance as

$$\dot{\psi}_{R} \le \boldsymbol{T}_{R}\cdot\dot{\boldsymbol{F}} + \mu\dot{c}_{R} - \boldsymbol{j}_{R}\cdot\nabla\mu. \tag{32}$$

Next, using (9) and (24), the stress-power $\boldsymbol{T}_{R}\cdot\dot{\boldsymbol{F}}$ admits the decomposition,

§ The fluid–solid mixture is treated as a single homogenized continuum body which allows for a mass flux of the fluid.

$$\boldsymbol{T}_{\mathrm{R}}:\dot{\boldsymbol{F}} = (\boldsymbol{T}_{\mathrm{R}}^{(1)} + \boldsymbol{T}_{\mathrm{R}}^{(2)}):\dot{\boldsymbol{F}}, \tag{33}$$

which may be recast in the form

$$\boldsymbol{T}_{\mathrm{R}}:\dot{\boldsymbol{F}} = \frac{1}{2}\boldsymbol{T}^{\mathrm{e}(1)}:\dot{\boldsymbol{C}}^{\mathrm{e}(1)} + \boldsymbol{M}^{\mathrm{e}(1)}:\boldsymbol{L}^{\mathrm{s}} + \frac{1}{2}\boldsymbol{T}^{\mathrm{e}(2)}:\dot{\boldsymbol{C}}^{\mathrm{e}(2)} + \boldsymbol{M}^{\mathrm{e}(2)}:\boldsymbol{L}^{\mathrm{v}}. \tag{34}$$

where

$$\boldsymbol{T}^{\mathrm{e}(\alpha)} \overset{\mathrm{def}}{=} J\boldsymbol{F}^{\mathrm{e}(\alpha)-1}\boldsymbol{T}^{(\alpha)}\boldsymbol{F}^{\mathrm{e}(\alpha)-\top} \tag{35}$$

and

$$\boldsymbol{M}^{\mathrm{e}(\alpha)} \overset{\mathrm{def}}{=} J\boldsymbol{F}^{\mathrm{e}(\alpha)\top}\boldsymbol{T}^{(\alpha)}\boldsymbol{F}^{\mathrm{e}(\alpha)-\top} \tag{36}$$

for each micromechanism $\alpha = \{1,2\}$.

Closely following our previous work[14] it can be shown that in order to satisfy thermodynamic restrictions the stresses and chemical potential are determined by the state relations

$$\boldsymbol{T}^{(1)} = J^{-1}\left(2\boldsymbol{F}^{\mathrm{e}(1)}\frac{\partial\psi_{\mathrm{R}}}{\partial\boldsymbol{C}^{\mathrm{e}(1)}}\boldsymbol{F}^{\mathrm{e}(1)\top}\right), \tag{37}$$

$$\boldsymbol{T}^{(2)} = J^{-1}\left(2\boldsymbol{F}^{\mathrm{e}(2)}\frac{\partial\psi_{\mathrm{R}}}{\partial\boldsymbol{C}^{\mathrm{e}(2)}}\boldsymbol{F}^{\mathrm{e}(2)\top}\right), \tag{38}$$

$$\mu = \frac{\partial\psi_{\mathrm{R}}}{\partial c_{\mathrm{R}}} + v\overline{p}, \tag{39}$$

where we have defined the mean normal pressure

$$\overline{p} \overset{\mathrm{def}}{=} -\frac{1}{3}J^{\mathrm{s}-1}\left(\mathrm{tr}\ \boldsymbol{M}^{\mathrm{e}(1)}\right).$$

Lastly, the dissipation inequality is given by

$$\boldsymbol{M}^{\mathrm{e}(2)}:\boldsymbol{L}^{\mathrm{v}} - \boldsymbol{j}_{\mathrm{R}}\cdot\nabla\mu \geq 0. \tag{40}$$

Here from (40) we can clearly observe the contribution to the total dissipation from both fluid permeation, and viscous effects.

5 Constitutive theory

We assume that the free energy density per unit reference volume is separable and given by

$$\psi_{\mathrm{R}} = \psi_{\mathrm{R}}^{(1)} + \psi_{\mathrm{R}}^{(2)} \tag{41}$$

where $\psi_{\mathrm{R}}^{(1)}$ and $\psi_{\mathrm{R}}^{(2)}$ are the free energy densities of micromechanism 1 and 2, respectively. In what follows we describe each individually and combine them later to obtain the full constitutive response.

5.1 Constitutive equations for micromechanism 1

Since micromechanism 1 closely follows our previous work,[14] for brevity we only present the major results here. We begin by assuming that the free energy $\psi^{(1)}$ may be written in the form[37]

$$\psi_{\mathrm{R}}^{(1)} = \mu^0 c_{\mathrm{R}} + \psi_{\mathrm{R,mixing}}(c_{\mathrm{R}}) + \psi_{\mathrm{R,mechanical}}(\boldsymbol{C}^{\mathrm{e}(1)},c_{\mathrm{R}}) \tag{42}$$

where μ^0 is the chemical potential of the unmixed pure solvent, $\psi_{\mathrm{R,mixing}}(c_{\mathrm{R}})$ is the change in free energy due to mixing of the solvent with the polymer network, and $\psi_{\mathrm{R,mechanical}}(\boldsymbol{C}^{\mathrm{e}(1)},c_{\mathrm{R}})$ is the contribution to the change in the free energy due to the deformation of the polymer network.

Estimate for $\psi_{\mathrm{R,mixing}}$

In the literature on swelling of elastomers, the quantity

$$\phi \overset{\mathrm{def}}{=} (1 + vc_{\mathrm{R}})^{-1} = (\lambda^{\mathrm{s}})^{-3} = J^{\mathrm{s}-1}, \quad 0 < \phi \leq 1, \tag{43}$$

is called the *polymer volume fraction*. Note that *the dry state corresponds to* $\phi = 1$, *and* $\phi < 1$ *represents a swollen state*. Next, following Doi[8,36] we adopt the following form of the Flory[34]–Huggins[35] theory for the contribution to the free energy due to mixing

$$\psi_{\mathrm{R,mixing}} = \frac{R\vartheta}{v}\frac{1}{\phi}\big((1-\phi)\ln(1-\phi) + \chi\phi(1-\phi)\big), \tag{44}$$

where R is the universal gas constant, ϑ the absolute temperature, and χ is a dimensionless parameter (called the χ-parameter, or interaction parameter), which represents the dis-affinity between the polymer and the fluid. If χ is increased, the fluid molecules are expelled from the gel and the gel shrinks, while if χ is decreased, the gel swells. The expression (44) for the mixing energy when expressed in terms of c_{R} is

$$\psi_{\mathrm{R,mixing}}(c_{\mathrm{R}}) = R\vartheta c_{\mathrm{R}}\left(\ln\left(\frac{vc_{\mathrm{R}}}{1+vc_{\mathrm{R}}}\right) + \chi\left(\frac{1}{1+vc_{\mathrm{R}}}\right)\right). \tag{45}$$

Estimate for $\psi_{\mathrm{R,mechanical}}$

In elastomeric materials, the major part of $\psi_{\mathrm{R,mechanical}}$ arises from an entropic contribution. Let

$$\overline{\lambda} \overset{\mathrm{def}}{=} \frac{1}{\sqrt{3}}\sqrt{\mathrm{tr}\ \boldsymbol{C}} = \frac{1}{\sqrt{3}}\sqrt{(1+vc_{\mathrm{R}})^{2/3}\mathrm{tr}\ \boldsymbol{C}^{\mathrm{e}(1)}} \tag{46}$$

define an *effective total stretch*. Then, classical non-Gaussian statistical mechanics models of rubber elasticity which take chain locking into account[46–49] provide the following estimate for the entropy change due to mechanical stretching

$$\eta_{\mathrm{R,mechanical}} = -N_{\mathrm{R}}k_{\mathrm{B}}\lambda_{\mathrm{L}}^2\left[\left(\frac{\overline{\lambda}}{\lambda_{\mathrm{L}}}\right)\beta + \ln\left(\frac{\beta}{\sinh\beta}\right) - \left(\frac{1}{\lambda_{\mathrm{L}}}\right)\beta_0 - \ln\left(\frac{\beta_0}{\sinh\beta_0}\right)\right] + N_{\mathrm{R}}k_{\mathrm{B}}\left(\frac{\lambda_{\mathrm{L}}}{3}\beta_0\right)\ln J, \tag{47}$$

with

$$\beta \overset{\mathrm{def}}{=} \mathscr{L}^{-1}\left(\frac{\overline{\lambda}}{\lambda_{\mathrm{L}}}\right), \text{and } \beta_0 \overset{\mathrm{def}}{=} \mathscr{L}^{-1}\left(\frac{1}{\lambda_{\mathrm{L}}}\right), \tag{48}$$

where $\mathscr{L}^{-1}$ is the inverse of the Langevin function $\mathscr{L}(x) = \coth(x) - (x)^{-1}$. This functional form for the change in entropy involves two material parameters: N_{R}, the number of polymer chains per unit reference volume, and λ_{L}, the *network locking stretch*.

Next, we take $\psi_{\mathrm{R,mechanical}}$ to also have an energetic component

$$\varepsilon_{\mathrm{R}} = \frac{1}{2}K\left(\ln J^{\mathrm{e}(1)}\right)^2, \tag{49}$$

where K is the bulk modulus of the gel. This is a contribution meant to reflect changes in the internal energy associated with volumetric mechanical deformation of the swollen elastomer.

Then, using (47) through (49), and writing

$$G_0 \overset{\text{def}}{=} N_R k_B \vartheta, \tag{50}$$

for a temperature dependent *ground-state shear modulus*, we obtain the estimate

$$\psi_{R,\text{mechanical}}\left(\boldsymbol{C}^{e(1)}, c_R\right) = G_0\lambda_L^2\left[\left(\frac{\bar{\lambda}}{\lambda_L}\right)\beta + \ln\left(\frac{\beta}{\sinh\beta}\right) - \left(\frac{1}{\lambda_L}\right)\beta_0 - \ln\left(\frac{\beta_0}{\sinh\beta_0}\right)\right] - G_0\left(\frac{\lambda_L}{3}\beta_0\right)\ln J + \frac{1}{2}K\left(\ln J^{e(1)}\right)^2. \tag{51}$$

5.2 Constitutive equations for micromechanism 2

The spectral representation of $\boldsymbol{C}^{e(2)}$ is

$$\boldsymbol{C}^{e(2)} = \sum_{i=1}^{3}\left(\lambda_i^{e(2)}\right)^2 \boldsymbol{r}_i^e \otimes \boldsymbol{r}_i^e \tag{52}$$

where $(\boldsymbol{r}_1^e,\boldsymbol{r}_2^e,\boldsymbol{r}_3^e)$ are the orthonormal eigenvectors of $\boldsymbol{C}^{e(2)}$ and $\boldsymbol{U}^{e(2)}$, and $(\lambda_1^{e(2)},\lambda_2^{e(2)},\lambda_3^{e(2)})$ are the eigenvalues of $\boldsymbol{U}^{e(2)}$. Let

$$\boldsymbol{E}^e \overset{\text{def}}{=} \sum_{i=1}^{3}\ln\left(\lambda_i^{e(2)}\right)\boldsymbol{r}_i^e \otimes \boldsymbol{r}_i^e \tag{53}$$

denote the logarithmic elastic strain. We take the free energy $\psi_R^{(2)}$ in the form

$$\psi_R^{(2)} = G_v\left|\boldsymbol{E}_0^e\right|^2 \tag{54}$$

where G_v is the shear modulus in micromechanism 2, and $\boldsymbol{E}_0^e$ is the deviatoric elastic strain. Implicitly stated in (54), is that we have assumed that micromechanism 2 does not contribute to the volumetric response of the gel, and all the volumetric response of the material occurs in micromechanism 1. This assumption is driven by the fact that in the absence of fluid the model presented here reduces to a simple, nearly incompressible viscoelastic rubber-like material. Nearly incompressible rubber-like materials are a class of materials where viscous effects are dominantly assumed to manifest in the deviatoric and not the volumetric response of the material (*e.g.*, Chapter 6, Section 10 in Hozapfel[50] and references therein).

The evolution equation for $\boldsymbol{F}^v$ is

$$\dot{\boldsymbol{F}}^v = \boldsymbol{D}^v\boldsymbol{F}^v \tag{55}$$

with the viscous stretching given by

$$\boldsymbol{D}^v = \dot{\gamma}^v\left(\frac{\boldsymbol{M}_0^{e(2)}}{2\bar{\tau}}\right), \tag{56}$$

where $\boldsymbol{M}^{e(2)}$ is the driving stress for viscous flow (typically referred to as the Mandel stress in the plasticity literature). Motivated by the standard linear solid of linear viscoelasticity (4), here for simplicity, the flow rule for the equivalent viscous shear strain $\dot{\gamma}^v$ rate is taken to be linearly viscous

$$\dot{\gamma}^v = \frac{\bar{\tau}}{\nu}, \tag{57}$$

with ν the shear viscosity, and $\bar{\tau}$ the equivalent shear stress given by

$$\bar{\tau} = \sqrt{(1/2)\boldsymbol{M}_0^{e(2)}:\boldsymbol{M}_0^{e(2)}}. \tag{58}$$

After simplification, we find that for this simple flow rule the viscous stretching is given by

$$\boldsymbol{D}^v = \frac{1}{2\nu}\boldsymbol{M}_0^{e(2)}, \tag{59}$$

and we define the characteristic relaxation time for this model as

$$t_r \overset{\text{def}}{=} \nu/G_v. \tag{60}$$

5.3 Fluid flux

We assume that the constitutive equation for the fluid flux obeys a "Darcy-type" relation. That is, the fluid flux $\boldsymbol{j}_R$ depends *linearly* on the chemical potential gradient $\nabla\mu$,

$$\boldsymbol{j}_R = -m\nabla\mu, \tag{61}$$

where m is the mobility.

5.4 Total free energy. Stress. Chemical potential

Thus, using (45), (51), and (54), in (42) and (41), a simple form of the free energy function which accounts for the combined effects of mixing, swelling, elastic stretching, and viscous effects, is

$$\psi_R = \mu^0 c_R + R\vartheta c_R\left(\ln\left(\frac{\upsilon c_R}{1+\upsilon c_R}\right) + \chi\left(\frac{1}{1+\upsilon c_R}\right)\right) + G_0\lambda_L^2\left[\left(\frac{\bar{\lambda}}{\lambda_L}\right)\beta + \ln\left(\frac{\beta}{\sinh\beta}\right) - \left(\frac{1}{\lambda_L}\right)\beta_0 - \ln\left(\frac{\beta_0}{\sinh\beta_0}\right)\right] - G_0\left(\frac{\lambda_L}{3}\beta_0\right)\ln J + \frac{1}{2}K\left(\ln J^{e(1)}\right)^2 + G_v\left|\boldsymbol{E}_0^e\right|^2. \tag{62}$$

Hence, we find that the Cauchy stress tensor is given by

$$\boldsymbol{T} = J^{-1}\left[G_0(\zeta\boldsymbol{B} - \zeta_0\mathbf{1}) + K\left(\ln J^{e(1)}\right)\mathbf{1} + 2G_v\tilde{\boldsymbol{E}}_0^e\right]. \tag{63}$$

where

$$G \overset{\text{def}}{=} G_0\zeta, \text{ with } \zeta \overset{\text{def}}{=} \left(\frac{\lambda_L}{3\bar{\lambda}}\right)\mathscr{L}^{-1}\left(\frac{\bar{\lambda}}{\lambda_L}\right), \text{ and } \zeta_0 \overset{\text{def}}{=} \left(\frac{\lambda_L}{3}\right)\mathscr{L}^{-1}\left(\frac{1}{\lambda_L}\right), \tag{64}$$

is a *generalized shear modulus*. Note that since $\mathscr{L}^{-1}(z) \to \infty$ as $z \to 1$, the stretch-dependent shear modulus $G \to \infty$ as $(\bar{\lambda}/\lambda_L) \to 1$. Also, we have used the notation $\tilde{\boldsymbol{E}}_0^e = \boldsymbol{R}^{e(2)}\boldsymbol{E}_0^e\boldsymbol{R}^{e(2)\top}$, or in other words $\tilde{\boldsymbol{E}}^e = \ln \boldsymbol{V}^{e(2)}$. Hence the Piola stress, $\boldsymbol{T}_R = J\boldsymbol{T}\boldsymbol{F}^{-\top}$, is given by

$$\boldsymbol{T}_R = G_0[\zeta\boldsymbol{F} - \zeta_0\boldsymbol{F}^{-\top}] + K(\ln J^{e(1)})\boldsymbol{F}^{-\top} + 2G_v\tilde{\boldsymbol{E}}_0^e\boldsymbol{F}^{-\top}. \tag{65}$$

Further, the stress $\boldsymbol{M}^{e(2)}$ which drives viscous flow in branch 2 is given by

$$\boldsymbol{M}^{e(2)} = 2G_v\boldsymbol{E}_0^e, \tag{66}$$

and we note that this stress is symmetric and deviatoric. And lastly, the chemical potential μ is given by

$$\mu = \mu^0 + R\vartheta(\ln(1-\phi) + \phi + \chi\phi^2) - \nu K(\ln J^{e(1)})\phi. \tag{67}$$

Remark: For a theory based on Gaussian statistics for configurational changes in entropy (also known as a Neo-Hookean model), the generalized shear modulus is no longer stretch-dependent, so that $G = G_0$, and the expression (63) for the stress, reduces to

$$\boldsymbol{T} = J^{-1}[G_0(\boldsymbol{B} - 1) + K(\ln J^{e(1)})1 + 2G_v\tilde{\boldsymbol{E}}_0^e], \tag{68}$$

while the expression (67) for the chemical potential remains unchanged.

6 Governing partial differential equations. Boundary conditions

The governing partial differential equations consist of

1. The local force balance for the macroscopic Piola stress,

$$\mathrm{Div}\ \boldsymbol{T}_R + \boldsymbol{b}_R = 0, \tag{69}$$

with $\boldsymbol{T}_R$ given by (65).

2. Use of (61) in the balance eqn (27) for the fluid content gives

$$\dot{c}_R = \mathrm{Div}(m\nabla\mu), \tag{70}$$

which, using (43), may be written in the form

$$\frac{\dot{\phi}}{\nu\phi^2} = -\mathrm{Div}(m\nabla\mu), \tag{71}$$

in which $m > 0$ is the fluid mobility, and the chemical potential μ is given by (67).

We also need initial and boundary conditions to complete the theory. Let $\mathscr{S}_\chi$ and $\mathscr{S}_t$ be complementary subsurfaces of the boundary ∂B of the body B in the sense $\partial\mathrm{B} = \mathscr{S}_\chi \cup \mathscr{S}_t$ and $\mathscr{S}_\chi \cap \mathscr{S}_t = \emptyset$. Similarly let $\mathscr{S}_\mu$ and $\mathscr{S}_j$ be complementary subsurfaces of the boundary: $\partial\mathrm{B} = \mathscr{S}_\mu \cup \mathscr{S}_j$ and $\mathscr{S}_\mu \cap \mathscr{S}_j = \emptyset$. Then for a time interval $t \in [0,T]$ we consider a pair of boundary conditions in which the motion is specified on $\mathscr{S}_\chi$ and the surface traction on $\mathscr{S}_t$:

$$\left.\begin{aligned} \chi &= \breve{\chi} \text{ on } \mathscr{S}_\chi \times [0,T], \\ \boldsymbol{T}_R\boldsymbol{n}_R &= \breve{\boldsymbol{t}}_R \text{ on } \mathscr{S}_t \times [0,T]; \end{aligned}\right\} \tag{72}$$

a pair of boundary conditions in which the chemical potential is specified on $\mathscr{S}_\mu$ and the fluid flux on $\mathscr{S}_j$

$$\left.\begin{aligned} \mu &= \breve{\mu} \text{ on } \mathscr{S}_\mu \times [0,T]; \\ -m(\nabla\mu)\cdot\boldsymbol{n}_R &= \breve{j} \text{ on } \mathscr{S}_j \times [0,T], \end{aligned}\right\} \tag{73}$$

with $\breve{\chi}$, $\breve{\boldsymbol{t}}_R$, $\breve{\mu}$, and $\breve{j}$ *prescribed* functions of $\boldsymbol{X}$ and t. The initial data is taken as

$$\boldsymbol{\chi}(\boldsymbol{X},0) = \boldsymbol{\chi}_0(\boldsymbol{X}) \text{ and } \mu(\boldsymbol{X},0) = \mu_0(\boldsymbol{X}) \text{ in B}. \tag{74}$$

The coupled set of eqn (69) and (71) together with (72), (74) and (75) yield an initial/boundary-value problem for the motion $\boldsymbol{\chi}(\boldsymbol{X},t)$, and the chemical potential $\mu(\boldsymbol{X},t)$.

In applications, for the case in which the environment consists of a pure and incompressible liquid, the boundary condition on chemical potential $\breve{\mu}$ is given by

$$\breve{\mu} = \mu^0 + p_a v, \tag{75}$$

where μ^0 is a reference chemical potential for the liquid, p_a is the hydrostatic pressure of the liquid, and v is the volume of a mole of liquid molecules. Also, if a portion of the boundary is impermeable to the liquid, then on that portion the prescribed normal flux $\breve{j}$ vanishes.

We have previously numerically implemented our deformation–diffusion theory in the commercial finite element program Abaqus/Standard[38] by writing special four-noded isoparametric quadrilateral plane-strain (UPE4) and axisymmetric (UAX4) user-elements, along with an eight-noded isoparametric continuum brick (U3D8) user-element which couple mechanical deformation and fluid permeation. In our numerical implementation we neglect body forces. Details of the numerical implementation are provided in Chester and Anand[14] and Chester.[51]

7 Applications

7.1 Further constitutive specializations. Representative values of material parameters

We begin by specifying a special form for the mobility function m. As in our previous work, we assume that the mobility function may be written in a separable form as follows,

$$m = \frac{D}{vR\vartheta}\gamma, \quad D > 0, \quad \gamma = \hat{\gamma}(\phi) > 0, \tag{76}$$

in which D represents a *diffusion coefficient* for the solvent molecules, and the dimensionless quantity $\gamma = \hat{\gamma}(\phi)$ represents a change in the mobility of solvent molecules as the polymer network is "opened" by an increase in the local fluid content. Here, for simplicity, we assume a linear dependence of the mobility on the polymer volume fraction

$$\gamma = (1 - \gamma_s)\phi + \gamma_s, \ \gamma_s > 1, \tag{77}$$

such that in the fully swollen state $\phi = 0$, the mobility is γ_s times its "dry" value.

Table 1 lists plausible values for the material properties of a viscoelastic polymeric gel at a temperature of 298 K.¶ Specifically, the ground state shear modulus for the polymer, G_0, is chosen to have a value 0.1 MPa, and the locking stretch is taken to have a value $\lambda_L = 2.5$. To model near incompressibility, the value of the bulk modulus K is taken to be 100 times higher than that of G_0. Additionally, we have chosen a value of $\chi = 0.1$ for the Flory–Huggins interaction parameter—a value which is

¶ We note that the constitutive theory is not meant to model any one particular system, but rather a class of materials/solvents, specifically gels that exhibit viscoelastic effects as well as fluid permeation. For that reason the material parameters are representative values in the appropriate physical range and specific to a particular material/solvent.

Table 1 Material parameters for a representative viscoelastic polymeric gel

Parameter	Value
N_R	2.43×10^{25} m^{-3}
$G_0 = N_R k_B \vartheta$ (at 298 K)	0.1 MPa
λ_L	2.5
K	10 MPa
χ	0.1
D	5×10^{-9} m^2 s^{-1}
γ_s	10
G_v	1 MPa
t_r	1×10^4 s
$\nu = G_v t_r$	10 GPa s

favorable for a high degree of swelling. The parameters (D,γ_s) for the mobility of fluid molecules are as listed in Table 1. Concerning the solvent, we set its reference chemical potential to $\mu^0 = 0.0$ J mol^{-1}, and the volume of a mole of solvent molecules is taken as

$$\upsilon = 1.7 \times 10^{-28}\ \text{m}^3 \equiv 100\ \text{cm}^3\ \text{mol}^{-1}.$$

For the material parameters related to the viscous micromechanism, for the shear modulus we assume $G_v = 1$ MPa. We have taken G_v much larger than G_0 such that at sort times the driving stresses for viscoelasticity are large corresponding to a large amount of relaxation. Further, since typical relaxation times for indentation of gels are measured on the time scale of hours (*cf. i.e.*, Hu *et al.*[23]) we assume a relaxation time $t_r = 1 \times 10^4$ seconds, with the corresponding viscosity $\nu = G_v t_r = 10.0$ GPa s as shown in Table 1. This choice allows for comparison of between elastic and viscoelastic indentation force relaxation curves in the case when relaxation times for fluid permeation and viscosity are roughly on the same scale—a situation where experimental results may be the most difficult to interpret.

7.2 Simple compression of a swollen gel

In this first example, we examine the displacement-controlled stress relaxation in simple compression of a finite-dimensioned swollen gel immersed in a fluid. Recently the competition between diffusion of solvent and viscous effects in gels has been mentioned in the literature.[24,27] Although the recent work of Zhao *et al.*[27] focuses on differences between the stress-relaxation of ionic and covalently crosslinked gels, and Hu *et al.*[24] is within the context of indentation, the key ingredient which applies here is that solvent diffusion has a characteristic time scale based on the specimen geometry and the diffusivity, whereas viscoelasticity does not depend on the geometry. Therefore, the mechanically measurable behavior such as load-deflection will be distinct for specimens of varying size due to the diffusion of the solvent, and not viscoelastic effects.

In what follows, we perform simple compression simulations on specimens of different sizes. In one case, we consider a compression specimen in the form of a right circular cylinder with an initial dry height and radius of $H_0 = R_0 = 1$ mm, and in another case an initial dry height and radius of $H_0 = R_0 = 5$ mm. Due to the symmetry of the problem, we model only an axisymmetric slice of the geometry. For simplicity, we consider frictionless contact between the compression platens and the gel, and further that the platens are impermeable to fluid. A schematic of the geometry and boundary conditions is shown in Fig. 2.

Regarding the initial conditions, the dry gel is initially taken to be stress free, at a temperature $\vartheta_0 = 298$ K, and a chemical potential $\mu_0 = -14\,388.57$ J mol^{-1} (computed using (67) with $\phi = 0.999$ and $J^{e(1)} = 1$). The dry gel is then swollen freely (*i.e.*, stress free and constraint free) to equilibrium such that $\mu = \mu^0$ everywhere inside the body. This equilibrium swollen configuration corresponds to $\phi_s = 0.1049$ with a swelling stretch of $\lambda_s = 2.121$, corresponding to $R = 2.121$ mm and $R = 10.6$ mm for the two specimens. After the equilibrium free swelling, the body is placed between compression platens, all the while still immersed in fluid. The compression is accomplished by translating the top platen downward over 60 seconds to a maximum displacement, and then holding that displacement constant for 24 hours. The deformation of the body during compression is prescribed by the axial stretch λ_2 as a function of time. We use

$$\lambda_2 = \begin{cases} \lambda_s \left[1 - 0.25 \left(\dfrac{t}{60} \right) \right] & \text{for } t \le 60 \text{ seconds} \\ 0.75 \lambda_s & \text{for } t > 60 \text{ seconds} \end{cases}$$

such that the displacement is linearly ramped from the equilibrium swelling position down to a reduced height of 75% of the equilibrium swollen height over 60 seconds and then held fixed for the remaining 24 hours. Referring to Fig. 2, the boundary conditions for displacement, tractions, chemical potential, and fluid flux are given by

- On the symmetry line (edge AD): $x_1 = X_1$, $-\nabla\mu \cdot \boldsymbol{e}_1 = 0$.
- On the outer surface (edge BC): $\boldsymbol{T}_R\, \boldsymbol{e}_1 = 0$, $\mu = \mu^0$.
- On the lower face (edge AB): $x_2 = X_2$, $-\nabla\mu \cdot \boldsymbol{e}_2 = 0$.
- On the upper face (edge CD): $x_2 = \lambda_2 X_2$, $-\nabla\mu \cdot \boldsymbol{e}_2 = 0$.

Lastly, due to the deformation field and boundary conditions, we assume that the polymer volume fraction is only a function of x_1, and that the material is elastically incompressible (*i.e.*, $\det \boldsymbol{F}^{e(1)} = 1$). These combined assumptions allow for a simple one dimensional boundary value problem to be solved numerically.

Fig. 3 shows the stress $T_{22} = T_{22}^{(1)} + T_{22}^{(2)}$, along with the individual contributions from each micromechanism $T_{22}^{(1)}$, and $T_{22}^{(2)}$, on the platen as a function of time for both cases $R_0 = 1$ mm and $R_0 = 5$ mm. The key result from this example is that for different

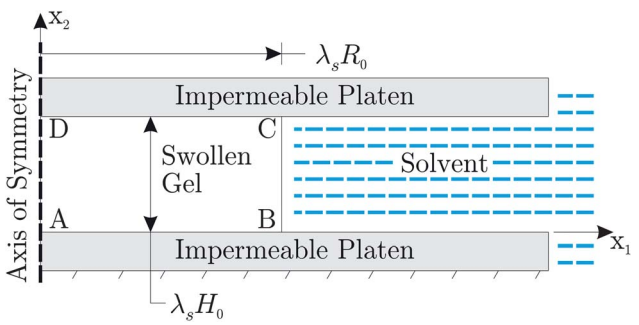

Fig. 2 Schematic of the simple compression geometry. The initial dry gel has a height of H_0 and radius of R_0, after free swelling the dimensions of the swollen gel are $H = \lambda_s H_0$ and $R = \lambda_s R_0$, with λ_s the swelling stretch.

sized specimens, the total observed stress relaxation behavior is different, however the contribution to the stress from micro-mechanism 2 is identical for both specimens. As expected, testing specimens of different sizes is one way to experimentally try to separate the effects of fluid permeation and mechanical dissipation in the "macroscopically apparent" time dependent phenomena observed in gels.

It is worth noting that the compression of a swollen gel is not a trivial exercise. After free swelling, the effective stretch $\bar{\lambda} = 2.121$, and from Table 1 the locking stretch is $\lambda_L = 2.5$, thus from free swelling alone, the material is at 85% of full extension. Then a fast (relative to the characteristic diffusion time) application of compressive strain does not allow adequate time for the fluid to exude from the body and the effective stretch will quickly approach the locking stretch under a moderately small *macroscopically apparent* compressive strain relative to the swollen gel. Therefore, one may expect compression specimens to experimentally damage and fail under such loading conditions as $\bar{\lambda}$ quickly approaches λ_L. A relatively slow application of the strain would allow for larger strains to be reached experimentally as time is allowed for fluid to leave the body. Additionally, viscoelastic effects may not be present depending on the time scale.

7.3 Three-dimensional indentation to a fixed depth

Recently, indentation of gels has received a lot of attention in the literature.[23–26] Primarily, these researchers have used experimentally measured force–relaxation curves from indentation experiments to estimate the elastic constants and a permeability coefficient which arise within the context (of a variant) of Biot's theory of *linear poroelasticity*.[20] In the recent work of Hu *et al.*[24] indentation experiments are reported that show a viscoelastic relaxation time on the order of tens of seconds compared to fluid permeation which takes on the order of hours. That disparity of relaxation times serves as the basis of their argument that viscoelasticity is not important when compared to fluid permeation in describing the observed force relaxation in PDMS swollen by solvent. However, it is well-known that dry PDMS does not exhibit a significant amount of viscoelasticity.[52,53] Other materials, such as silica gels which are known to be viscoelastic,[15] or chloroprene rubber which is known to be viscoelastic in the absence of solvent[54] may still exhibit viscoelasticity that persists even after swelling. In this example, we examine the displacement-controlled indentation of a finite-dimensioned swollen gel, which is immersed in a fluid, with a cylindrical rigid indenter. The indentation is carried out to a fixed depth, and the subsequent relaxation of the indentation force is monitored. We examine the case where viscoelastic effects are on the same time scale as fluid permeation (a situation where experimental results may be the most difficult to interpret), as well as a few cases of varying viscoelastic relaxation times (including when viscoelasticity is negligible) for comparison.

A schematic of the geometry for the indentation simulation is shown in Fig. 4. The initially dry, rectangular-shaped specimen has a lateral dimension of $W_0 = 20$ mm and initial height $H_0 = 10$ mm, the rigid impermeable cylindrical indenter has a radius of $R = 10$ mm. Due to symmetry of the problem, we model only one-quarter of the geometry as indicated in Fig. 4 with 1000 U3D8 elements. In order to avoid numerical problems, the indenter edge is given a small fillet radius of 1 mm.

The simulation is carried out in two steps:

1. In the first step, the fluid is allowed to diffuse into the dry gel for 72 hours.

2. In the second step the cylindrical indenter is displaced 5 mm downward into the swollen gel over a period of 60 seconds, after which the displacement is held constant for a total period of 6 hours. The reaction force on the cylindrical indenter is monitored during the complete indentation and hold period.

Referring to Fig. 4, the other boundary conditions are as follows:

• For the mechanical boundary conditions, the nodes along symmetry planes of the rectangular block of gel are prescribed

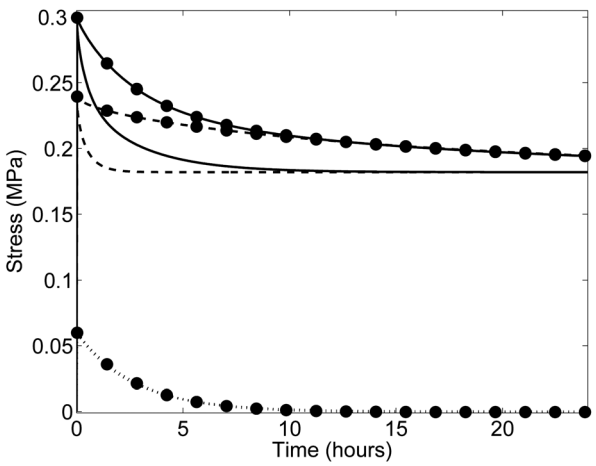

Fig. 3 Stress as a function of time in simple compression. Here curves marked by • correspond to the $R_0 = 5$ mm case, while unmarked curves correspond to the $R_0 = 1$ mm case. For both cases, the elastic (and coupled with fluid permeation) component of stress $T_{22}^{(1)}$ is given by dashed lines, the viscous component of stress $T_{22}^{(2)}$ by the dotted lines, and lastly the total stress T_{22} by the solid lines. Note that the viscous component of stress $T_{22}^{(2)}$ for $R_0 = 1$ mm and $R_0 = 5$ mm lie directly on top of each other.

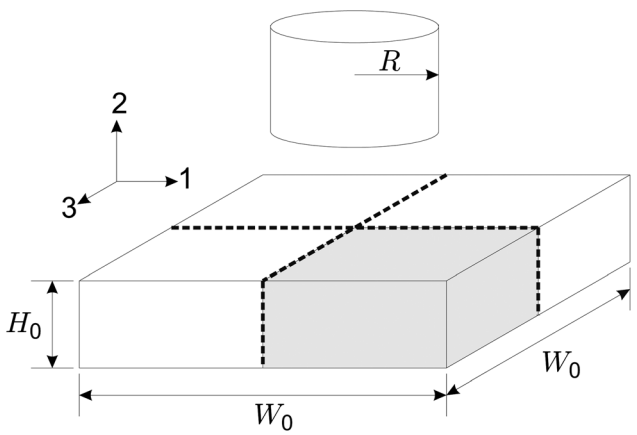

Fig. 4 Schematic of the initial geometry for the indentation simulation. The thick dashed-lines indicate the symmetry planes; the finite element calculation is performed only for the portion of the body shown in grey.

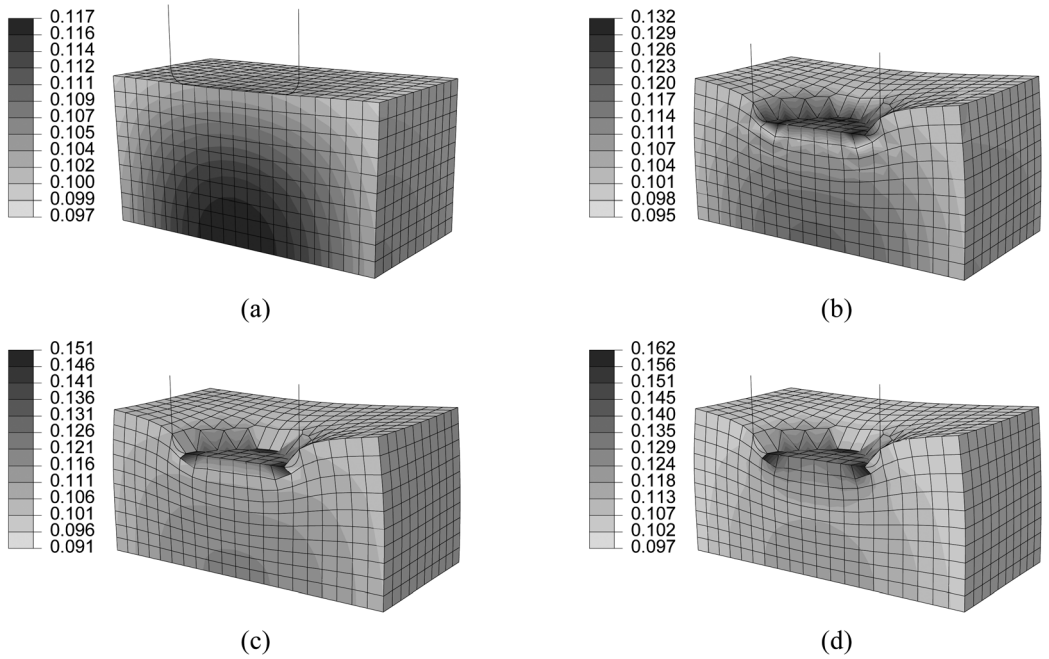

Fig. 5 Contours of the polymer volume fraction ϕ after (a) 72 hours of free swelling; and then after indentation with an impermeable cylindrical punch at (b) 60 seconds, (c) 10 minutes, and (d) 6 hours. Here the mesh as been mirrored about one of the symmetry planes and only the outline of the punch shown for clarity. Note the change in scale for the contours of ϕ for each time. The contours of the polymer volume fraction are nearly the same for all cases simulated, consequently we only show the case for $t_r = \infty$ s.

appropriate displacement conditions, while nodes located on the bottom of the gel ($X_2 = 0$) are prescribed $u_2 = 0$. All other surfaces of the gel are traction free. The cylindrical indenter is prescribed $u_1 = u_3 = 0$ with u_2 the prescribed displacement as described in the prior paragraph. Contact between the gel and the cylindrical indenter is assumed frictionless.

• In the first swelling step, for the chemical boundary conditions, the symmetry planes of the gel, and the bottom of the gel, are prescribed a zero fluid flux, whereas on the remaining surfaces of the gel, the chemical potential is set to be $\breve{\mu}(t) = \mu^0$, where μ^0 is the chemical potential of the ambient solvent.

• For the second indentation step, all symmetry planes and the bottom of the gel are prescribed a zero fluid flux. We consider a *impermeable* indenter so that the fluid cannot pass through the indenter. Accordingly, we prescribe a zero fluid flux on the portion of the surface of the gel which is in contact with the cylindrical indenter.‖ Lastly, we prescribe $\breve{\mu} = \mu^0$ on all remaining surfaces.

Regarding the initial conditions, the gel is taken to be stress free, at a temperature $\vartheta_0 = 298$ K, and a chemical potential $\mu_0 = -14\,388.57$ J mol^{-1}. We run all simulations with $G_v = 1$ MPa as given in Table 1, while varying t_r from 10 s all the way to $t_r = \infty$ s (effectively fully elastic) for comparison.

Fig. 5a shows the deformed gel and contours of the polymer volume fraction, ϕ, at the end of the swelling step—after 72 hours of free swelling the gel has a lateral dimension of $W \approx 40$ mm and a height of $H \approx 20$ mm, and the polymer volume fraction is roughly $\phi \approx 0.1$. Fig. 5b–d show the indented gel and contours of the polymer volume fraction at 60 seconds, 10 minutes, and 6 hours, respectively, for the case of $t_r = \infty$ s. In these figures the mesh has been mirrored about one symmetry plane, and the rigid indenter has been removed for clarity. Further, since the contours of ϕ are nearly identical for all simulations we only show results for $t_r = \infty$ sec. Finally, Fig. 6 shows the variation of the reaction force on the rigid indenter as a function of time. The relaxation of the indenter force at a fixed indentation depth is due to (i) the fluid being expelled from the gel, and (ii) viscoelastic stress relaxation.

The recent work of Hu *et al.*[24] relates the experimental indentation response to the elastic constants in a fully elastic, elastically incompressible, Flory–Huggins theory for polymeric gels. Their analysis assumes the indentation to be a small perturbation on the fully swollen equilibrated state, and after some analysis the elastic constants are computed using nothing more than indentation experiments. However, for a theory such as this one that includes nonlinear diffusion and viscous effects, indentation experiments alone may not be sufficient to fully determine the material parameters. For example, γ_s from (77), is most easily obtained from an instrumented swelling experiment such as that of Achilleos *et al.*,[30] after the elastic constants have been obtained. Further, in the absence of fluid the model presented here reduces to a simple, nearly incompressible viscoelastic rubber-like material. Therefore standard testing techniques for that class of materials can identify all but the diffusion related material parameters, which may then be obtained using indentation or other experimental techniques.

‖ Due to the complex contact conditions, the zero fluid flux boundary condition is prescribed at the start of the indentation step, over all element faces that *will* contact the indenter tip. It is a reasonable approximation since the displacement occurs over 60 seconds compared to the full 6 hour simulation time. Further, the solvent diffuses on a time scale $\sim R^2/D$, which in this particular case is on the order of hours.

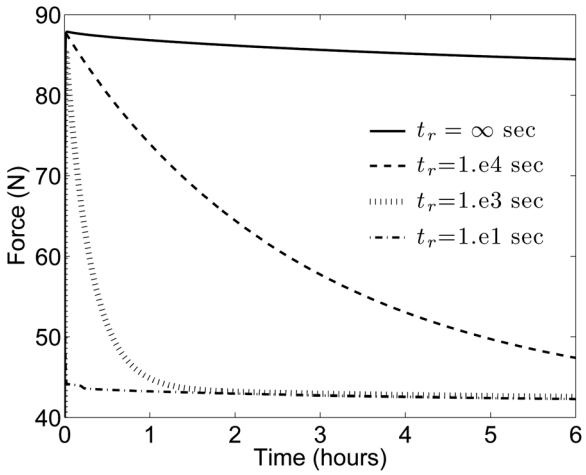

Fig. 6 Reaction force on the rigid indenter as a function of time for various values of relaxation times in micromechanism 2 at a fixed $G_v = 1$ MPa.

8 Concluding remarks

We have presented a continuum mechanical theory to describe coupled fluid permeation and large viscoelastic deformations in non-ionic polymeric gels. We have implemented the theory in the finite element package Abaqus/Standard[38] by using a specialized user element subroutine (UEL). We have shown this theory able to simulate the qualitative behavior shown in compression and indentation of polymeric gels.

Time dependent phenomena in gels may be attributed to a variety of mechanisms such as fluid squeezing out of the gel, viscous effects in the underlying polymeric network, a combination of both, and so on. From a constitutive modeling point of view, the theory presented here can qualitatively account for those effects. However, the main difficultly still lies in determination of specific constitutive forms and the accompanying material parameters from experiments. Looking toward the future, the ability to separate the effects of each of these such micromechanisms from experimental results would lead to vasty improved, and even more importantly, predictive constitutive models.

Acknowledgements

The author thanks Lallit Anand (Massachusetts Institute of Technology) for many fruitful discussions and for the use of computational hardware and software. Part of this work was performed under the auspices of the U.S. Department of Energy by Lawrence Livermore National Laboratory under Contract DE-AC52-07NA27344.

References

1 T. Tanaka and D. Fillmore, *J. Chem. Phys.*, 1979, **70**, 1214–1218.
2 C. Durning and K. Morman, *J. Chem. Phys.*, 1993, **98**, 4275–4293.
3 S. Baek and A. Srinivasa, *Int. J. Non Lin. Mech.*, 2004, **39**, 201–218.
4 J. Dolbow, E. Fried and H. Ji, *J. Mech. Phys. Solids*, 2004, **52**, 51–84.
5 H. Ji, H. Mourad, E. Fried and J. Dolbow, *Int. J. Solids Struct.*, 2005, **43**, 1878–1907.
6 V. Korchagin, J. Dolbow and D. Stepp, *Int. J. Solids Struct.*, 2007, **44**, 3973–3997.
7 W. Hong, X. Zhao, J. Zhou and Z. Suo, *J. Mech. Phys. Solids*, 2008, **56**, 1779–1793.
8 M. Doi, *J. Phys. Soc. Jpn.*, 2009, **78**, 052001.
9 F. Duda, A. Souza and E. Fried, *J. Mech. Phys. Solids*, 2010, **58**, 515–529.
10 S. Baek and T. Pence, *J. Mech. Phys. Solids*, 2011, **59**, 561–582.
11 S. Cai and Z. Suo, *J. Mech. Phys. Solids*, 2011, **59**, 2259–2278.
12 F. Duda, A. Souza and E. Fried, *J. Mech. Phys. Solids*, 2011, **59**, 2341–2354.
13 S. Chester and L. Anand, *J. Mech. Phys. Solids*, 2010, **58**, 1879–1906.
14 S. Chester and L. Anand, *J. Mech. Phys. Solids*, 2011, **59**, 1978–2006.
15 G. Scherer, S. Pardenek and R. Swiatek, *J. Non-Cryst. Solids*, 1988, **107**, 14–22.
16 G. Scherer, *J. Non-Cryst. Solids*, 1989, **109**, 171–182.
17 G. Scherer, *J. Non-Cryst. Solids*, 1989, **113**, 107–118.
18 G. Scherer, *J. Non-Cryst. Solids*, 1992, **142**, 18–35.
19 G. Scherer, *Langmuir*, 1996, **12**, 1109–1116.
20 M. Biot, *J. Appl. Phys.*, 1941, **12**, 155–164.
21 C. Hui, Y. Lin, F. Chuang, K. Shull and W. Lin, *J. Polym. Sci., Part B: Polym. Phys.*, 2006, **43**, 359–370.
22 S. Cai, Y. Hu, X. Zhao and Z. Suo, *J. Appl. Phys.*, 2010, **108**, 113514.
23 Y. Hu, X. Zhao, J. Vlassak and Z. Suo, *Appl. Phys. Lett.*, 2010, **96**, 121904.
24 Y. Hu, X. Chen, G. Whitesides, J. Vlassak and Z. Suo, *J. Mater. Res.*, 2011, **26**, 785–795.
25 Y. Hu, E. P. Chan, J. J. Vlassak and Z. Suo, *J. Appl. Phys.*, 2012, **110**, 086103.
26 Y. Hu, J.-O. You, D. T. Auguste, Z. Sho and J. J. Vlassak, *J. Mater. Res.*, 2012, **27**, 152–160.
27 X. Zhao, N. Huebsch, D. Mooney and Z. Suo, *J. Appl. Phys.*, 2010, **107**, 063509.
28 Q. Liu, G. Subhash and D. Moore, *J. Mech. Behav. Biomed. Mater.*, 2011, **4**, 974–982.
29 J. Yoon, S. Cai and Z. Suo, *Soft Matter*, 2010, **6**, 6004–6012.
30 E. Achilleos, R. Prud'homme, K. Christodoulou, K. Gee and I. Kevrekidis, *Chem. Eng. Sci.*, 2000, **55**, 3335–3340.
31 J. Gong, Y. Katsuyama, T. Kurokawa and Y. Osada, *Adv. Mater.*, 2003, **15**, 1155–1158.
32 X. Wang and W. Hong, *Soft Matter*, 2011, **7**, 8576–8581.
33 X. Zhao, *J. Mech. Phys. Solids*, 2012, **60**, 319–332.
34 P. Flory, *J. Chem. Phys.*, 1942, **10**, 51–61.
35 M. Huggins, *J. Phys. Chem.*, 1942, **46**, 151–158.
36 M. Doi, *Introduction to Polymer Physics*, Clarendon Press, Oxford, 1996.
37 P. Flory, *Principles of Polymer Chemistry*, Cornell University Press, Ithaca, 1953.
38 *Abaqus/Standard*, SIMULIA, Providence, RI, 2010.
39 M. Gurtin, E. Fried and L. Anand, *The Mechanics and Thermodynamics of Continua*, Cambridge University Press, Cambridge, 2010.
40 L. Anand, N. Ames, V. Srivastava and S. Chester, *Int. J. Plast.*, 2009, **25**, 1474–1494.
41 N. Ames, V. Srivastava, S. Chester and L. Annad, *Int. J. Plast.*, 2009, **25**, 1495–1539.
42 V. Srivastava, S. Chester, N. Ames and L. Anand, *Int. J. Plast.*, 2010, **26**, 1138–1182.
43 V. Srivastava, S. Chester, N. Ames and L. Anand, *J. Mech. Phys. Solids*, 2010, **58**, 1100–1124.
44 M. Silberstein and M. Boyce, *J. Power Sources*, 2010, **195**, 5692–5706.
45 M. Silberstein and M. Boyce, *J. Power Sources*, 2011, **196**, 3452–3460.
46 L. Treloar, *The Physics of Rubber Elasticity*, Oxford University Press, Oxford, 1975.
47 E. Arruda and M. Boyce, *J. Mech. Phys. Solids*, 1993, **41**, 389–412.
48 L. Annad, *Comput. Mech.*, 1996, **18**, 339–355.
49 J. Bischoff, E. Arruda and K. Grosh, *Rubber Chem. Technol.*, 2001, **74**, 541–559.
50 G. Hozapfel, *Nonlinear Solid Mechanics a Continuum Approach for Engineering*, John Wiley & Sons, Chichester, 2001.
51 S. Chester, PhD thesis, Department of Mechanical Engineering, Massachusetts Institute of Technology, 2011.
52 S. Clarson and J. Semlyen, *Siloxane Polymers*, Prentice-Hall, Englewood Cliffs, 1993.
53 R. Huang and L. Anand, Non-linear mechanical behavior of the elastomer polydimethlysiloxane (PDMS) used in the manufacture of microfluidic devices, 2005, http://hdl.handle.net/1721.1/7456.
54 J. Bergstrom and M. Boyce, *J. Mech. Phys. Solids*, 1998, **46**, 931–954.